International Journal of Engineering Inventions
e-ISSN: 2278-7461, p-ISSN: 2319-6491
Volume 15, Issue 11 [November 2026] PP: 192-202

Integrated Ground Magnetic, Aeromagnetic and Aeroradiometric Interpretation for Mineral Exploration in Kabba, North-Central Nigeria

Adebimpe Agunbiade, Akaninyene O. Akankpo, Kufre Udoh, Promise James Akpan
Department of Physics, Faculty of Physical Sciences, University of Uyo, Uyo, Akwa Ibom State, Nigeria

Abstract— *Structurally controlled mineralisation in the Precambrian basement of North-Central Nigeria is difficult to target from surface geology alone because of deep weathering and sparse outcrop. This study integrates high-resolution airborne magnetic and radiometric data covering the north-western quadrant of Sheet 246 (Kabba), Kogi State, with a detailed ground magnetic survey in order to map lithological contrasts, structural controls and possible alteration zones. The airborne radiometric grids show potassium (K) of 0.34–3.40 %, equivalent thorium (eTh) of 6.06–24.52 ppm, equivalent uranium (eU) of 0.98–6.07 ppm and Th/K ratios of 2.56–38.98, with radioelement enrichment concentrated in the eastern, south-eastern and northern sectors. Residual total magnetic intensity (TMI) of −55.7 to 166.1 nT was enhanced with first and second vertical derivatives, tilt derivative and total horizontal derivative. A GEM-19 Overhauser magnetometer was used in the walking-magnetometer mode along 15 traverses spaced 100 m apart; the data were base-station corrected, gridded and processed through reduction to the equator, analytic signal, tilt, vertical and horizontal derivative filters. The results reveal a dominant NE–SW structural grain with subordinate NW–SE and E–W lineaments, three major faults, and dense lineament intersections in the central and southern parts of the area. The coincidence of magnetic highs, structural nodes and radioelement anomalies defines prioritised targets for iron-oxide, nickel–copper, vein-hosted and pegmatite-related mineralisation. The integrated approach reduces the non-uniqueness of single-method interpretation and provides a basis for induced polarisation, geochemical and drilling follow-up.*

Keywords— *Aeromagnetic data; aeroradiometric data; ground magnetic survey; lineaments; mineralisation; Kabba; Nigerian Basement Complex*

Date of Submission: 05-11-2026 Date of acceptance: 16-11-2026

I. INTRODUCTION

Solid-mineral exploration in Nigeria has increasingly relied on geophysics because the Precambrian Basement Complex, which underlies roughly half of the country, is deeply weathered and poorly exposed (Obaje, 2009; Rahaman, 1988). In such terrains, mineralisation is commonly controlled by faults, shear zones, lithological contacts and intrusive bodies, all of which have subtle surface expression but measurable physical-property contrasts at depth (Dentith & Mudge, 2014). Magnetic surveying responds to variations in the magnetic susceptibility and remanence of rocks, and is therefore widely used to map lithology, contacts and structure (Kearey et al., 2002; Telford et al., 1990). Airborne gamma-ray spectrometry complements it by mapping the near-surface concentrations of potassium, thorium and uranium, which reflect rock chemistry, magmatic differentiation, weathering and hydrothermal alteration (Dickson & Scott, 1997; International Atomic Energy Agency [IAEA], 2003).

Airborne surveys cover large areas quickly but are flown at a nominal terrain clearance and line spacing that limit their resolution of narrow, shallow targets. Ground magnetic surveys fill this gap by providing closely spaced, high-resolution measurements, while the airborne data supply the regional framework needed to place the ground observations in context. Several studies have shown that combining airborne magnetic, radiometric and ground or remote-sensing data yields more reliable structural and alteration maps than any single dataset (Akame et al., 2019; Elkhateeb & Abdellatif, 2018). Aeromagnetic interpretation has also been applied to structural and mineral-potential mapping in other parts of North-Central Nigeria (Abdulsalam et al., 2024; Tawey et al., 2020).

Magnetic interpretation is, however, inherently non-unique because of the dipolar nature of the field and the variety of magnetisation processes (Kearey et al., 2002; Reeves, 2005). The ambiguity can be reduced by constraining the interpretation with independent geological and geophysical information. This study therefore integrates aeromagnetic, aeroradiometric and ground magnetic data from the Kabba area with published geology

and field observations. The objectives are to (i) identify the structural trends in the area; (ii) delineate magnetic and radiometric anomalies and relate them to lithology; (iii) analyse the structural controls on mineralisation; and (iv) define priority targets for follow-up exploration.

II. STUDY AREA AND GEOLOGICAL SETTING

The airborne data cover the north-western quadrant of the 1:100,000 Kabba Sheet 246, Kogi State, approximately between longitudes 6°00′E and 6°15′E and latitudes 7°45′N and 8°00′N (UTM zone 32N, 170,000–196,000 mE and 860,000–885,000 mN; Fig. 1). The ground magnetic survey was carried out within this quadrant at about 6°02′–6°04′E and 7°50′–7°52′N, north-west of Kabba town. The terrain is undulating, with steep hills separated by lowlands; the Shuttle Radar Topography Mission (SRTM) elevation model shows elevations of about 277 m to 552 m above mean sea level, rising from the south towards the central and north-western parts (Fig. 1b). The area lies in the tropical climate zone, with alternating wet and dry seasons, and falls in the Southern Guinea Savanna–Northern Rainforest vegetation belt.

The area is part of the North-Central Nigerian Basement Complex, itself a segment of the Pan-African mobile belt located between the West African and Congo Cratons and south of the Tuareg Shield (Black, 1980; Obaje, 2009; Ajibade & Fitches, 1988). It lies within the Kabba–Lokoja–Igarra schist belt, where a migmatite–schist suite comprising migmatite gneiss, migmatised schist and a quartz–mica schist–quartzite complex is interbanded locally with amphibolite lenses; quartzite occurs as elongated ridges (Kolawole et al., 2017). Older granites, porphyroblastic gneiss and coarse porphyritic biotite and hornblende–biotite granite and granodiorite also occur (Fig. 2). The metamorphic sequence is intruded by north–south trending granite plutons associated with dolerite, pegmatite and aplite veins (Kolawole et al., 2017).

Kolawole et al. (2017) recognised at least two thermotectonic events in the Kabba–Bunu area: one with E–W fold axes produced by N–S compression, probably Eburnean in age, and another with N–S fold axes produced by E–W compression and associated with the Pan-African event. Foliation and lineation in the E–W to NE–SW directions are interpreted as the earlier ductile structures, while minor brittle shear structures trending NW–SE to N–S are filled by quartz veins, dolerites and pegmatite dykes. These brittle structures are considered conduits for gold-bearing and other ore-forming fluids (Kolawole et al., 2017), which makes the area a suitable test site for a structural-geophysical exploration approach.

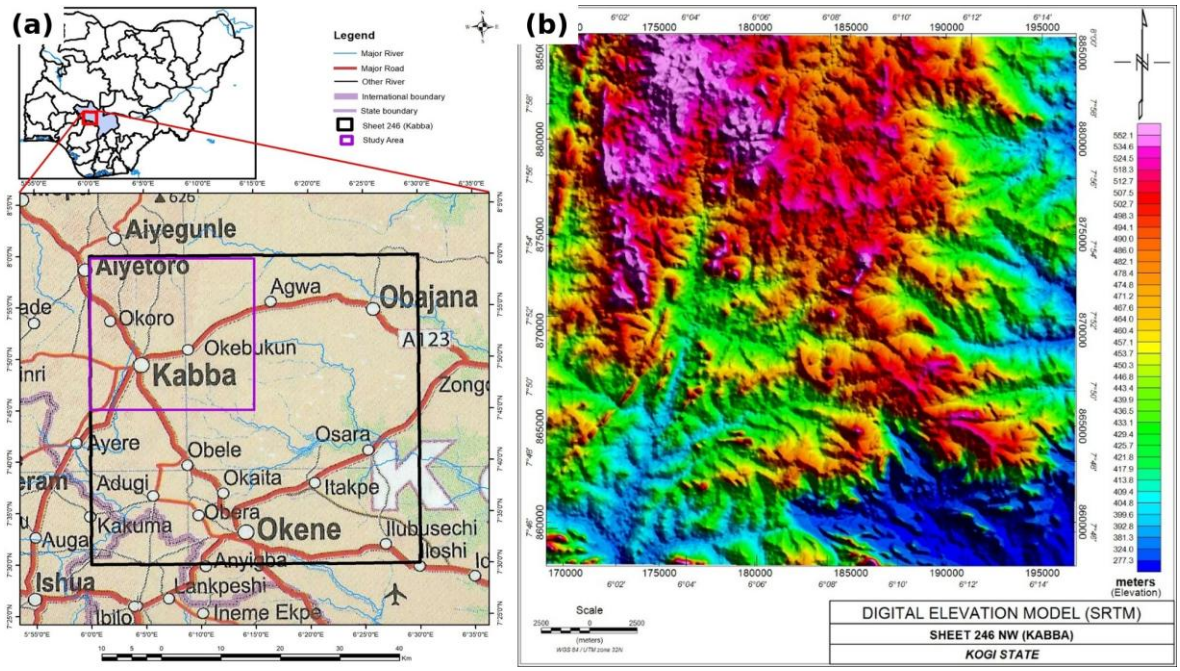


Fig. 1. Study area. (a) Location of the study area (purple box) within Sheet 246 (Kabba), Kogi State, North-Central Nigeria. (b) SRTM digital elevation model of Sheet 246 NW (Kabba). Source: Nigerian Geological Survey Agency (NGSA).

III. MATERIALS AND METHODS

A. Airborne Magnetic and Radiometric Data

The airborne magnetic and radiometric datasets of Sheet 246 (Kabba) were obtained from the Nigerian Geological Survey Agency (NGSA), which commissioned the nationwide high-resolution airborne survey flown by Fugro Airborne Services between 2003 and 2010 (NGSA, 2010). The radiometric grids of potassium (K, %),

equivalent thorium (eTh, ppm) and equivalent uranium (eU, ppm) were used to compute the Th/K ratio map and a ternary K–Th–U composite image. The residual total magnetic intensity (TMI) grid was subjected to standard enhancement filters in Oasis montaj: first vertical derivative (FVD), second vertical derivative (SVD), tilt derivative (TDR) and total horizontal derivative (THD) (Blakely, 1995; Miller & Singh, 1994; Verduzco et al., 2004). The derived maps were used to pick lineaments and to identify areas of anomalous response, which guided the siting of the ground traverses.

B. Ground Magnetic Survey

The ground survey was carried out with a GEM-19 Overhauser magnetometer (resolution 0.01 nT) operated in the walking-magnetometer (WALKMAG) mode, with the sensor back-pack mounted and readings recorded continuously at 2 s intervals. Fifteen traverses of 300 m to 1.2 km length were laid out with a 100 m line spacing having an area extent of 13 km, and station positions and elevations were recorded with a Garmin GPS76 receiver. A second magnetometer was installed as a fixed base station in a magnetically quiet location, away from vehicles and outcrops, to record the diurnal variation of the geomagnetic field, which can reach tens of nanoteslas per hour (Dobrin & Savit, 1988). Both instruments were tuned to a field of 33,000 nT. Quality control and assurance were applied through visual inspection of the raw profiles and field notes on geology, cultural features and noise sources.

Data were downloaded with GEM Link software, and compiled in spreadsheets. The reduced magnetic data for all profiles was put into a database for further two-dimensional processing and interpretation, using Geosoft Oasis Montaj software. After diurnal correction against the base-station record, the regional field was removed using the International Geomagnetic Reference Field (IGRF), and the residual data were gridded by minimum curvature (Briggs, 1974). Because the survey lies at low magnetic latitude, where anomalies are skewed and displaced from their sources, the TMI grid was reduced to the equator (RTE) (MacLeod et al., 1993; Reeves, 2005). The following filters were then applied to the RTE grid to enhance edges and structure: the analytic signal amplitude (Nabighian, 1972; Roest et al., 1992), the tilt derivative, the first and second vertical derivatives, and a directional horizontal derivative (135° from +X). The analytic signal amplitude, the tilt derivative and the total horizontal derivative are given by

$$|A| = \sqrt{[(\partial M/\partial x)^2 + (\partial M/\partial y)^2 + (\partial M/\partial z)^2]} \quad (1)$$

$$TDR = tan^{-1}\{(\partial M/\partial z) / \sqrt{[(\partial M/\partial x)^2 + (\partial M/\partial y)^2]}\} \quad (2)$$

$$THD = \sqrt{[(\partial M/\partial x)^2 + (\partial M/\partial y)^2]} \quad (3)$$

where M is the magnetic field. The analytic signal is independent of the direction of magnetisation, which makes it particularly useful at low latitudes (MacLeod et al., 1993; Roest et al., 1992).

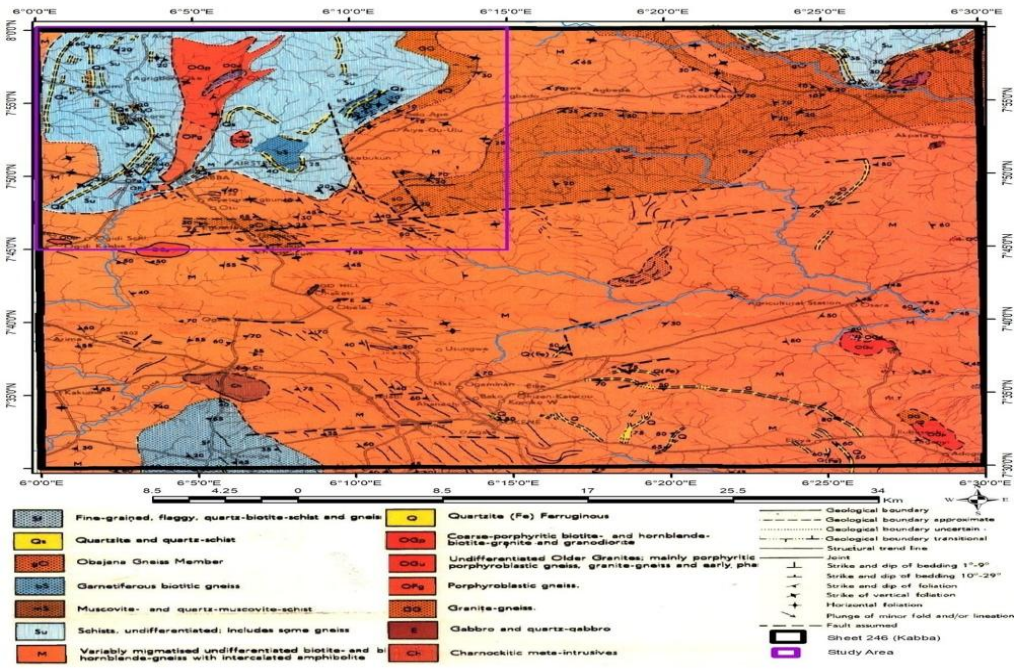


Fig. 2. Geological map of Sheet 246 (Kabba) showing the study area (purple box). Source: NGSA (2008).

The tilt derivative equalises the response of shallow and deep sources, and its zero contour approximates the edges of the causative bodies (Miller & Singh, 1994; Salem et al., 2008). Lineaments, faults and magnetic unit

boundaries were digitised in ArcGIS to produce the structural map and were compared with field observations of the NE–SW trending quartz schist and quartzite ridges.

IV. RESULTS AND DISCUSSION

The datasets and the ranges of values read from the map scales are summarised in Table I. The results are presented from the regional airborne data to the detailed ground data, followed by an integrated interpretation.

TABLE I. SUMMARY OF THE GEOPHYSICAL DATASETS USED IN THE STUDY

Dataset	Parameter (unit)	Range of values	Dominant spatial pattern
Airborne radiometric	Potassium, K (%)	0.34 – 3.40	High in the east, south-east and parts of the centre; low in the west and south-west
	Equivalent thorium, eTh (ppm)	6.06 – 24.52	High in the north, north-east and centre; low in the south
	Equivalent uranium, eU (ppm)	0.98 – 6.07	High in the north, north-east and centre; low in the south
	Th/K ratio	2.56 – 38.98	Low in the east and south-east (coincident with K highs); high in the west and north-centre
Airborne magnetic	Residual TMI (nT)	−55.7 to 166.1	Highs in the central-southern and south-western parts; lows in the north and north-east
Ground magnetic	Elevation (m)	428.7 – 487.7	Highest in the north and north-west; lowest in the south
	TMI (nT)	23,516 – 23,798	Elongated NE–SW high in the central-north-eastern part; lows in the south and south-east
	RTE-TMI (nT)	23,535 – 23,770	NE–SW high corridor in the north and centre; lows in the south and south-east

A. Airborne Radiometric Interpretation

The eU, eTh and K maps (Fig. 3) show a heterogeneous distribution of radioelements, which is characteristic of basement terrains and reflects lithological variation, magmatic differentiation and weathering (Dickson & Scott, 1997; IAEA, 2003). High eU and eTh concentrations occur mainly in the northern, north-eastern and central parts of the area, whereas the southern part is dominated by low values eU and eTh concentrations. Such enrichment is typical of evolved felsic rocks such as granites, pegmatites and migmatites, in which thorium and uranium are hosted by accessory minerals such as monazite, zircon, thorite and uraninite (IAEA, 2003; Dickson & Scott, 1997). The low eU and eTh values in the south are consistent with mafic lithologies, or with areas depleted by weathering and leaching under tropical conditions (Wilford et al., 1997).

Potassium shows a different pattern: high values are concentrated in the eastern, south-eastern and part of the central area, and low values in the west and south-west. The overlap of high K with moderately high eTh and eU in the east and south-east points to K-feldspar-, muscovite- and biotite-rich granitic and pegmatitic rocks. Because potassium is relatively mobile during hydrothermal alteration, K enrichment accompanied by a low Th/K ratio is a recognised indicator of potassic alteration (Dickson & Scott, 1997; Pirajno, 2009). In the study area the Th/K map (Fig. 3d) shows low ratios in the east and south-east, coincident with the K highs, and high ratios in the west and north-central part, where K is depleted relative to Th. The eastern K-enriched, low Th/K zone is therefore regarded as a possible alteration zone and is ranked as a target, although lithological enrichment in felsic intrusions cannot be excluded without ground sampling.

The ternary K–Th–U image (Fig. 4) integrates the three channels. Pink, red and whitish tones, indicating high concentrations of all three elements, dominate the eastern and south-eastern parts and are interpreted as evolved granitic and pegmatitic rocks. The central part is characterised by mixed green and cyan tones, reflecting transitional granitoid gneisses and migmatites, while the dark, subdued signatures of the western and north-western parts correspond to mafic to intermediate rocks or to intensely weathered basement. Sharp colour changes mark lithological boundaries and, together with the linear patterns in the K and eTh maps, suggest structural control on the emplacement of the felsic bodies (Wilford et al., 1997).

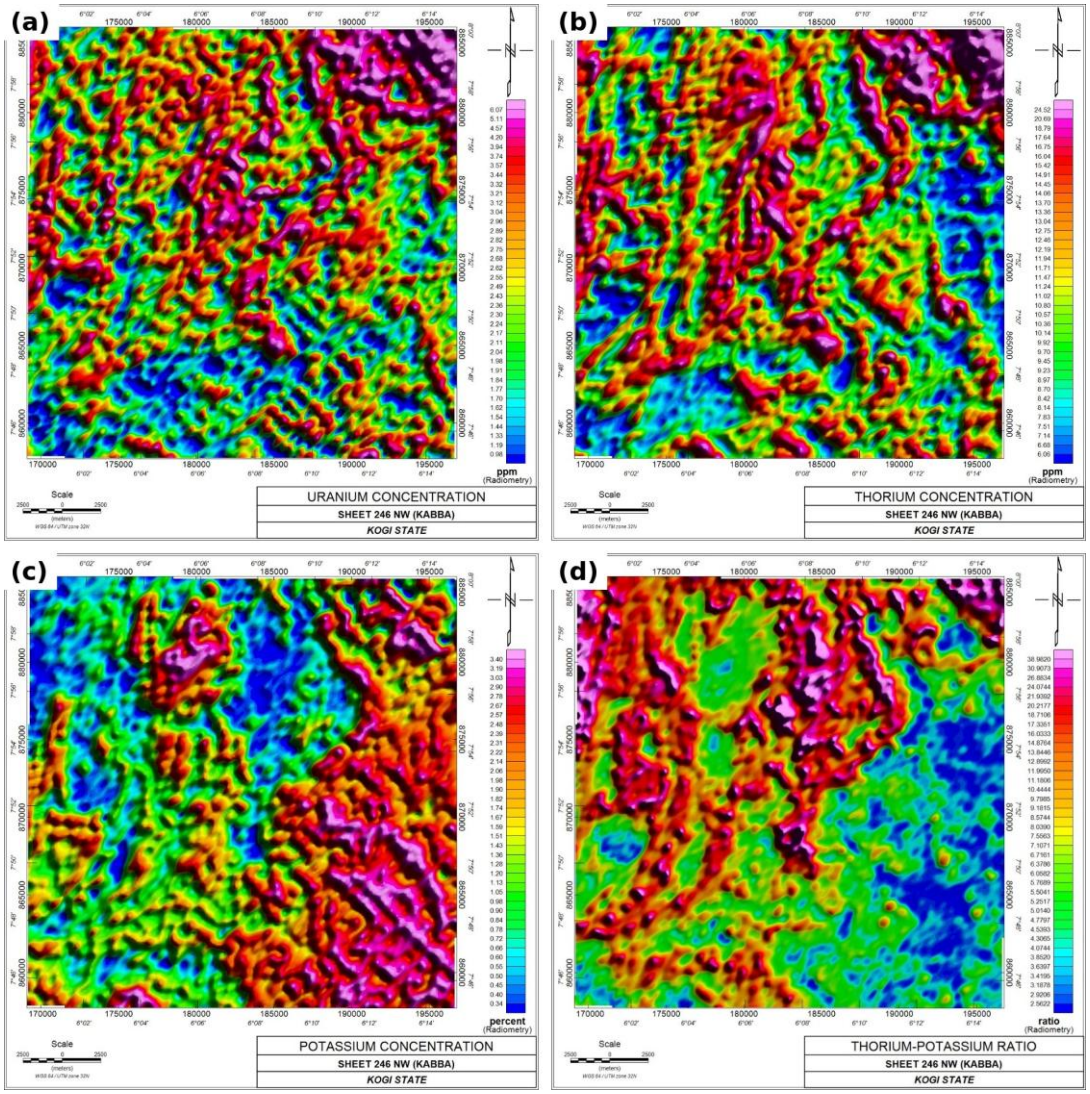


Fig. 3. Airborne radiometric maps of Sheet 246 NW (Kabba). (a) Equivalent uranium (ppm); (b) equivalent thorium (ppm); (c) potassium (%); (d) Th/K ratio. Source: NGSA.

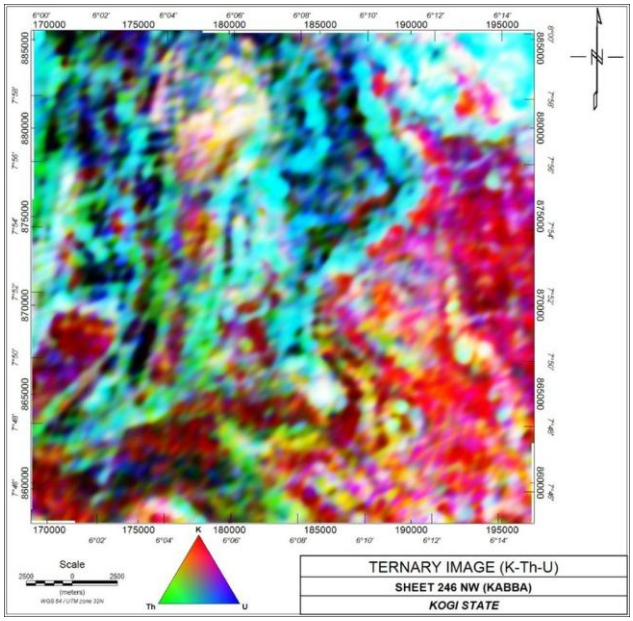


Fig. 4. Ternary K–Th–U radiometric image of Sheet 246 NW (Kabba). Source: NGSA

B. Aeromagnetic Interpretation

The residual TMI map (Fig. 5a) ranges from −55.7 to 166.1 nT and shows pronounced linear and broad anomalies with variable amplitudes and gradients. Magnetic highs are concentrated in the central-southern and south-western parts, and are interpreted as magnetite-bearing mafic and amphibolitic rocks, whereas magnetic lows in the north and north-east reflect demagnetised granitic rocks, weathered or altered basement and possibly thin cover. The anomalies are aligned predominantly NE–SW, with subordinate NW–SE and E–W trends forming a conjugate pattern of lineaments, which is consistent with the tectonic grain of the Nigerian Basement Complex (Odeyemi, 1988; Obaje, 2009). In the central-southern part, intersecting lineaments define probable highly fractured zones.

The derivative maps sharpen this structural picture. The FVD and SVD maps (Figs. 5c and 5d) are dominated by short-wavelength, high-gradient anomalies in the central-southern part of the area, indicating shallow sources and intensely deformed NE–SW fault zones; the north and north-east are characterised by smoother, low-amplitude responses, indicating comparatively undeformed or altered rocks. Vertical-derivative filters suppress regional trends and resolve closely spaced anomalies, so that the near-surface structures are emphasised (Kearey et al., 2002; Reeves, 2005). The tilt derivative (Fig. 5e) delineates elongated, continuous ridges that are interpreted as faults, shear zones, dyke swarms and lithological contacts, with a dominant NE–SW trend and a secondary E–W to ENE–WSW fabric. The coexistence of these orientations suggests polyphase deformation and reactivation during multiple tectonic events (Odeyemi, 1988; Obaje, 2009).

The THD map (Fig. 5b) shows numerous high-gradient lineaments, which mark source edges and are interpreted as contacts, faults, shears and intrusive boundaries (Blakely, 1995). The strongest and most closely spaced responses occur in the southern and south-western parts, indicating major fault corridors and strong susceptibility contrasts, whereas the northern and central areas have lower THD amplitudes with isolated high-gradient features. Structural intersections occur in the central and south-western sectors, and such nodes are favourable sites for fluid focusing and ore deposition (Groves et al., 2020). Magnetic highs are prospective for iron-oxide and nickel–copper mineralisation associated with mafic intrusions, while subdued magnetic corridors that follow lineament intersections may mark hydrothermal alteration, in which magnetite has been destroyed (Dentith & Mudge, 2014; Reeves, 2005).

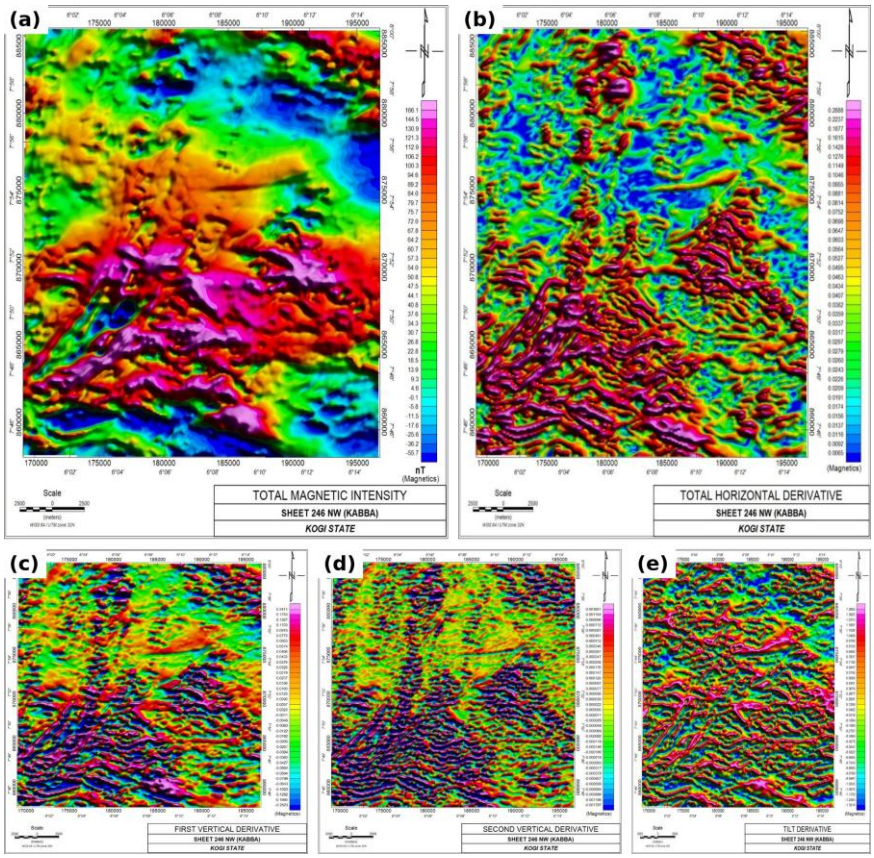


Fig. 5. Airborne magnetic maps of Sheet 246 NW (Kabba). (a) Residual total magnetic intensity (nT); (b) total horizontal derivative; (c) first vertical derivative; (d) second vertical derivative; (e) tilt derivative. Source: NGSA.

C. Ground Magnetic Interpretation

The ground elevation map (Fig. 6a) shows a topographic range of about 59 m over the survey block, with the highest ground in the north and north-west and the lowest in the south. The ground TMI map (Fig. 6b) shows pronounced variability (23,516–23,798 nT), suggesting a heterogeneous subsurface of rocks with contrasting magnetic properties. The highest values occur as an elongated NE–SW anomaly in the central and north-eastern part of the block, and the lowest in the south and south-east. The strong gradient along the margin of this high is interpreted as a major structural discontinuity, such as a fault, shear zone or lithological contact. Smaller linear trends elsewhere in the block indicate a structurally complex area that has undergone several deformation phases (Kolawole et al., 2017).

Reduction to the equator (Fig. 6c) repositions the anomalies closer to their sources and increases the clarity of the boundaries. The RTE-TMI map (23,535–23,770 nT) shows a NE–SW magnetic corridor of elongated highs and sharp gradients crossing the central part of the block, with a secondary NW–SE to E–W set of trends. The sharp transition between high and low domains reflects structural control and may mark a boundary between magnetically high rocks, interpreted as amphibolitic or magnetite-bearing metamorphic rocks, and lower-susceptibility units, interpreted as granitic, quartz-rich or weathered rocks (Dentith & Mudge, 2014; Reeves, 2005).

The analytic signal map (Fig. 6d) is independent of the magnetisation direction and has its maxima over the edges of magnetic bodies (Nabighian, 1972; Roest et al., 1992). High amplitudes form clusters in the central and southern parts of the block and in the north-east. They are interpreted as faults and fracture zones, lithological contacts and intrusive bodies, and indicate strong susceptibility contrasts along NE–SW and, to a lesser extent, NW–SE structures. Moderate amplitudes represent transitional or fractured and weathered basement, which may form alteration halos around the main structures, while the low-amplitude western areas indicate magnetically uniform or deeper sources. The sharpness of the high-amplitude anomalies in the central part of the block suggests that the magnetic sources there are shallow.

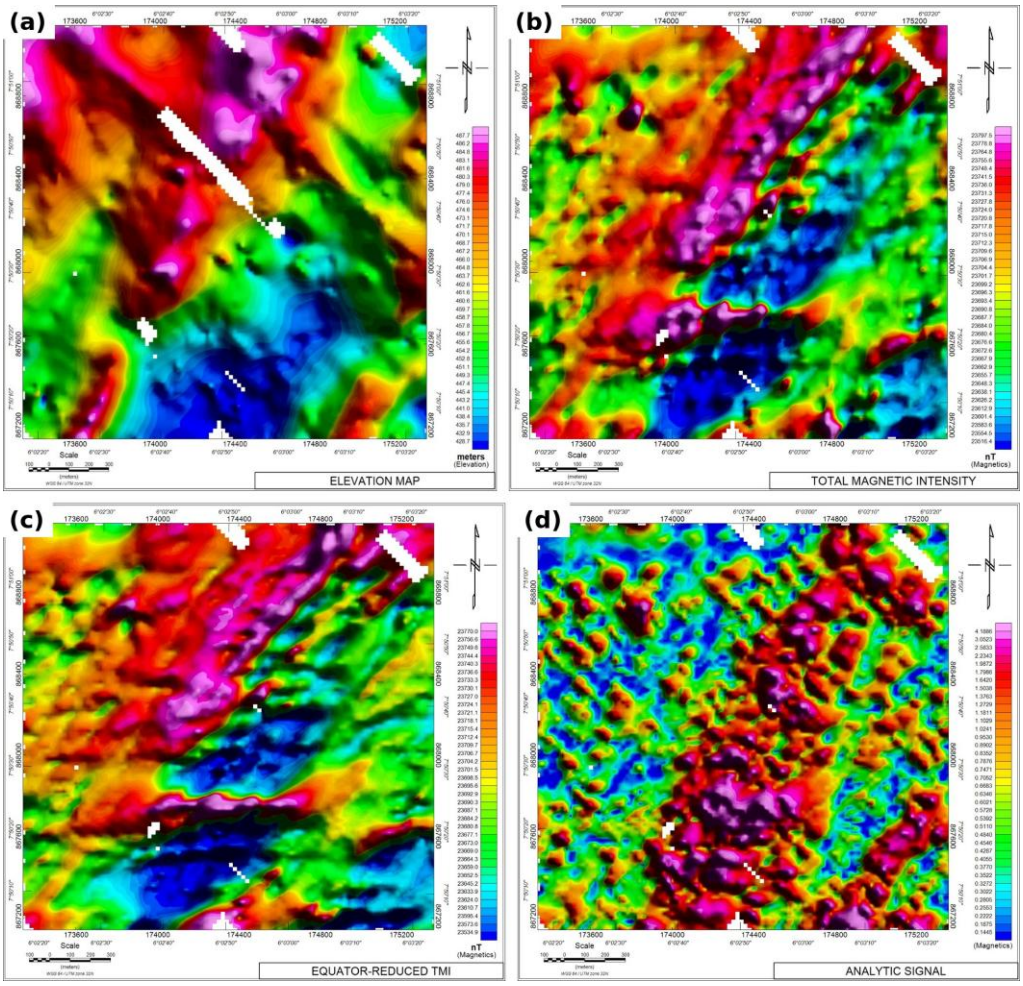


Fig. 6. Ground magnetic survey maps of the Kabba block. (a) Ground elevation (m); (b) total magnetic intensity (nT); (c) equator-reduced TMI (nT); (d) analytic signal amplitude.

The tilt derivative, FVD, SVD and horizontal derivative maps (Fig. 7) further resolve the structural fabric. The tilt derivative (Fig. 7a) shows continuous NE–SW lineaments with subsidiary E–W to ENE–WSW trends, and the intersections between them are potential zones of permeability and fluid flow. The FVD map (Fig. 7b) shows a dense network of linear and curvilinear anomalies, again dominated by NE–SW structures with minor NW–SE cross-cutting features. Contacts appear as narrow high-gradient zones, more sharply defined than on the tilt map, which confirms shallow, structurally controlled sources. The SVD map (Fig. 7c) is more fragmented but sharper still, reflecting its greater sensitivity to very shallow sources and minor fractures. The horizontal derivative map along 135° from +X (Fig. 7d) highlights the NE–SW trending fault and shear system as the primary tectonic fabric, with E–W and NW–SE structures cross-cutting it. A central NE–SW corridor appears to be a major zone of crustal weakness that may have acted as a pathway for magmatic and hydrothermal fluids (Odeyemi, 1988; Groves et al., 2020).

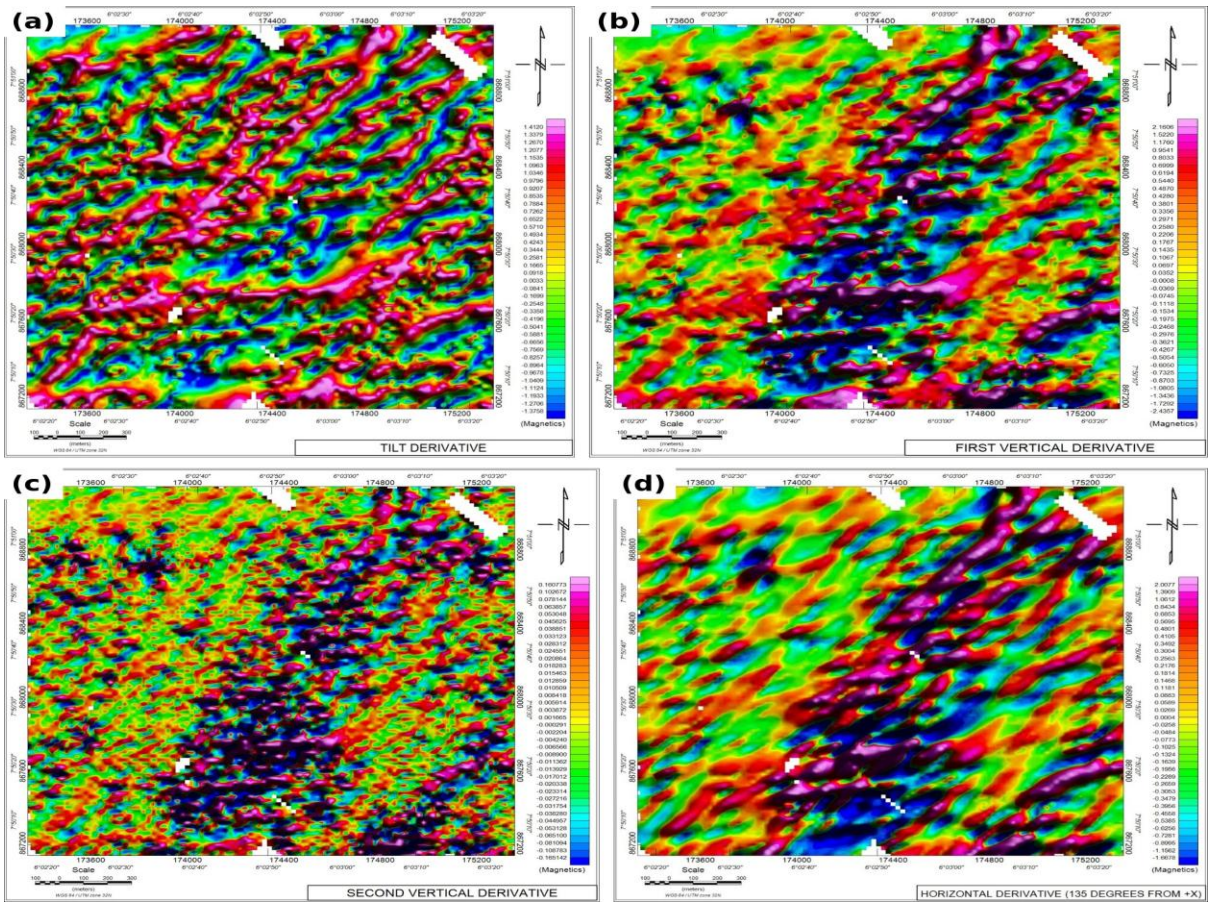


Fig. 7. Enhanced ground magnetic maps of the Kabba block. (a) Tilt derivative; (b) first vertical derivative; (c) second vertical derivative; (d) horizontal derivative (135° from +X).

D. Structural Map

Lineaments picked from the airborne and ground derivative maps were compiled into an interpreted structural map (Fig. 8). Structures were identified from offsets of similar magnetic units, abrupt discontinuities, and sudden changes in the depth to magnetic sources. The lineaments can be grouped into three sets by orientation: a dominant NE–SW set, and subordinate E–W and NW–SE sets. Three major faults were delineated, which intersect one another, the other lineaments and the magnetic unit boundaries. The shape of the magnetic signatures generally suggests step or edge structures, such as dykes or contacts, at depth. The map is in agreement with field observations of NE–SW trending structures in quartz schist and quartzite, and with the NE–SW positive aeromagnetic anomalies of the project area.

Cross-cutting relationships indicate three structural episodes: NE–SW structures, interpreted as the oldest; NW–SE structures; and a nearly N–S set, with the NNW–SSE and NNE–SSW structures being the youngest, which is consistent with the N–S trend of the Pan-African event that affected most of the country (Ajibade & Fitches, 1988; Kolawole et al., 2017). The fact that most structures can be mapped on the first vertical derivative indicates that they are not deeply buried.

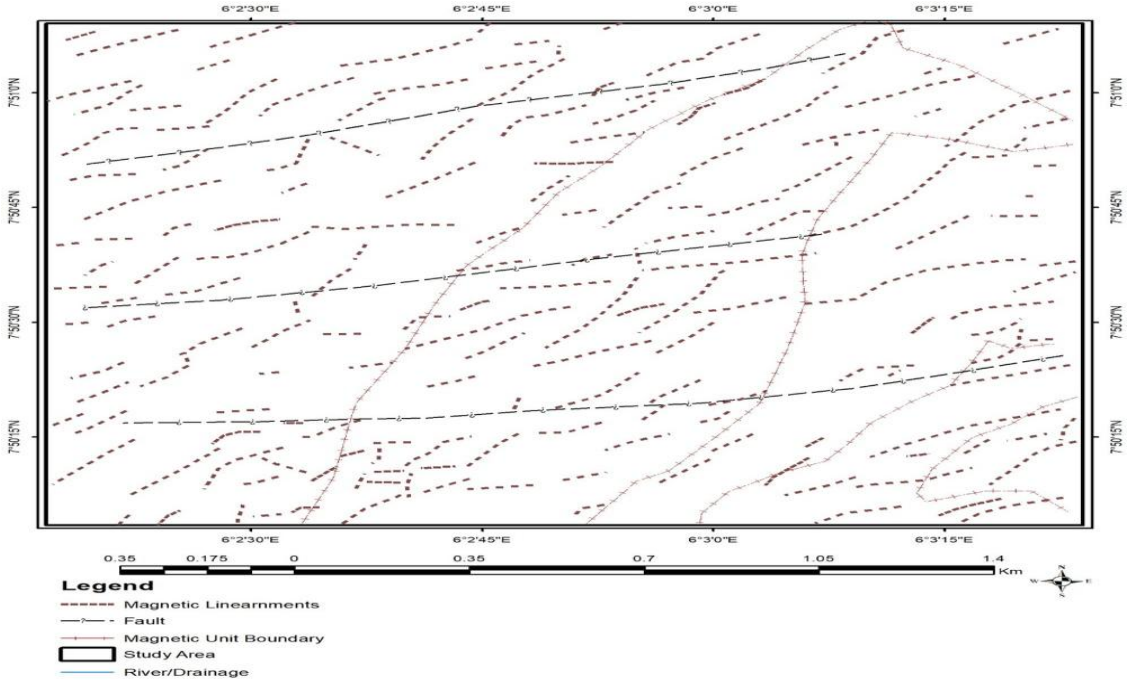


Fig. 8. Interpreted structural map of the Kabba ground survey block showing magnetic lineaments, faults, magnetic unit boundaries and drainage.

E. Integrated Interpretation and Exploration Targets

The airborne and ground datasets are consistent. The NE–SW dominant structural grain, the secondary NW–SE and E–W trends and the intersections that are pervasive in the central and southern sectors are evident on the TMI and on all derivative maps at both scales. The ground data refine the airborne picture by resolving shallow structures, such as the three major faults, that the regional grid can only show as broad trends. The magnetic and radiometric datasets also complement each other: magnetic highs mark magnetite-bearing mafic and amphibolitic rocks and the magnetic lows mark granitic, weathered or altered rocks, whereas the radiometric maps differentiate the felsic, K–Th–U enriched intrusions in the east and south-east from the less evolved rocks in the west and north-west. The coincidence of the radioelement anomalies with the magnetic structural trends indicates that emplacement and alteration were controlled by the same regional tectonic framework.

On this basis, mineralisation in the area is considered predominantly structurally controlled. The highest potential is where the major NE–SW fault and shear corridors intersect the secondary structural trends, because the resulting fractured zones favour hydrothermal fluid circulation and ore deposition (Groves et al., 2020; Kolawole et al., 2017). The proposed targets are summarised in Table II and are prioritised by the number of independent datasets that support them.

TABLE II. INTEGRATED INTERPRETATION AND PRIORITISED EXPLORATION TARGETS

Target zone	Geophysical expression	Inferred geology and mineral potential
1. Central–southern structural corridor	Magnetic highs on TMI; strong FVD, SVD and THD responses; high analytic-signal amplitudes; dense NE–SW lineaments crossed by NW–SE and E–W structures	Magnetite-bearing mafic and amphibolitic rocks with potential for iron-oxide and Ni–Cu mineralisation; structural nodes favourable for hydrothermal, vein-hosted mineralisation (Priority 1)
2. Kabba ground-survey block	NE–SW magnetic high bounded by steep gradients; three major faults intersecting lineaments and unit boundaries; shallow sources	Structurally controlled sulphide or quartz-vein mineralisation in shear zones; detailed follow-up with induced polarisation and geochemistry (Priority 1)
3. Eastern and south-eastern radioelement zone	High K, eTh and eU; low Th/K ratio; pink–white ternary signature	Evolved granitic and pegmatitic intrusions, possible potassic alteration; accessory Th–U minerals (monazite, zircon, allanite, uraninite) with rare-earth potential (Priority 2)
4. Northern and north-eastern domain	Magnetic lows with elevated eU and eTh	Demagnetised granitic or hydrothermally altered rocks; secondary target (Priority 3)
5. Western and north-western domain	Low radioelement concentrations; subdued analytic signal	Weathered mafic to intermediate basement or thicker cover; low priority

The aeromagnetic and radiometric data was used as a secondary data to interpret, delineate the geological features and terrain of the study area. On the other hand, ground magnetic survey was used to get direct interpretations for mineral exploration. This integrated method encounters some limitation since the radiometric signal represents only the uppermost tens of centimetres of the ground, so it may be affected by soil cover and weathering (IAEA, 2003), and magnetic interpretation remains non-unique, due to the facts that magnetic lows may reflect either alteration or lithology. In addition, the ground survey also covers a small part of the airborne area, due to facts that insecurity, difficult terrain and equipment costs restricted the extent of coverage. The targets in Table II are therefore prospective and require testing by additional methods.

V. CONCLUSION

Integrated interpretation of airborne magnetic, airborne radiometric and ground magnetic data from the Kabba area leads to the following conclusions:

- There exists a good relation between the aero magnetic, aero radiometric and ground magnetic survey data, showing delineated linear structures (anomaly zone) within the study area even as revealed by geological mapping and ground trothing previously done in the area.
- The area is a structurally complex Precambrian basement terrain dominated by NE–SW lineaments, with subordinate NW–SE, E–W and ENE–WSW trends that record polyphase deformation.
- Airborne and ground magnetic data are mutually consistent; the ground survey resolved shallow structures, including three major faults that intersect other lineaments and the magnetic unit boundaries.
- Magnetic highs are linked to magnetite-bearing mafic and amphibolitic rocks, while magnetic lows reflect granitic, weathered or altered rocks. The radiometric data discriminate felsic K–Th–U enriched rocks in the east and south-east from less evolved basement elsewhere, and a low Th/K ratio with high K indicates possible potassic alteration.
- Mineralisation is considered predominantly structurally controlled. The central-southern corridor and the ground-survey block, where structural intersections, high magnetic gradients and analytic-signal peaks coincide, are the priority targets, followed by the eastern radioelement-enriched zone.

It is recommended that induced polarisation imaging, especially toward the western part of the survey block where chargeable responses were recorded in test lines, and detailed geochemical sampling of rocks, soils and stream sediments be carried out and integrated with the present results before drilling.

ACKNOWLEDGMENT

The author thanks the Nigerian Geological Survey Agency (NGSA) for providing the airborne magnetic and radiometric datasets and the geological maps used in this study.

REFERENCES

[1]. Abdulsalam, N. N., Jegede, A., Egbelehulu, P., & Ibeneme, S. I. (2024). Delineation of mineralized zones in parts of University of Abuja main campus, Abuja, Nigeria from aeromagnetic data. Nigerian Journal of Physics, 33(3). https://doi.org/10.62292/njp.v33i3.2024.289

[2]. Ajibade, A. C., & Fitches, W. R. (1988). The Nigerian Precambrian and the Pan-African orogeny. In Precambrian geology of Nigeria (pp. 45–53). Geological Survey of Nigeria.

[3]. Akame, J. M., Assembe, S. P., Zo'o Zame, P., Owona, S., Ndougsa Mbarga, T., Azia, G. A., & Mvondo Ondoa, J. (2019). The integration of remote sensing and aeromagnetic data for structural interpretation in Sangmelima granite-greenstone belt, South Cameroon. The Egyptian Journal of Remote Sensing and Space Sciences, 22(1), 37–47.

[4]. Black, R. (1980). Precambrian of West Africa. Episodes, 1980(4), 3–8.

[5]. Blakely, R. J. (1995). Potential theory in gravity and magnetic applications. Cambridge University Press.

[6]. Briggs, I. C. (1974). Machine contouring using minimum curvature. Geophysics, 39(1), 39–48.

[7]. Dentith, M., & Mudge, S. T. (2014). Geophysics for the mineral exploration geoscientist. Cambridge University Press.

[8]. Dickson, B. L., & Scott, K. M. (1997). Interpretation of aerial gamma-ray surveys – adding the geochemical factors. AGSO Journal of Australian Geology and Geophysics, 17(2), 187–200.

[9]. Dobrin, M. B., & Savit, C. H. (1988). Introduction to geophysical prospecting (4th ed.). McGraw-Hill.

[10]. Elkhateeb, S. O., & Abdellatif, M. A. G. (2018). Delineation of potential gold mineralization zones in a part of Central Eastern Desert, Egypt using airborne magnetic and radiometric data. NRIAG Journal of Astronomy and Geophysics, 7(2), 361–376. https://doi.org/10.1016/j.nrjag.2018.05.010

[11]. Groves, D. I., Santosh, M., & Zhang, L. (2020). A scale-integrated exploration model for orogenic gold deposits based on a mineral system approach. Geoscience Frontiers, 11(3), 719–738. https://doi.org/10.1016/j.gsf.2019.12.007

[12]. International Atomic Energy Agency. (2003). Guidelines for radioelement mapping using gamma ray spectrometry data (IAEA-TECDOC-1363). IAEA.

[13]. Kearey, P., Brooks, M., & Hill, I. (2002). An introduction to geophysical exploration (3rd ed.). Blackwell Science.

[14]. Kolawole, M. S., Onimisi, M., & Olobaniyi, S. B. (2017). Field occurrence and structural characteristics of basement rocks around Kabba-Bunu Area in part of Kabba-Lokoja-Igarra Schist Belt, southwestern Nigeria. Global Journal of Pure and Applied Sciences, 23(2), 263–274. https://doi.org/10.4314/gjpas.v23i2.7

[15]. MacLeod, I. N., Jones, K., & Dai, T. F. (1993). 3-D analytic signal in the interpretation of total magnetic field data at low magnetic latitudes. Exploration Geophysics, 24(3–4), 679–688.

[16]. Miller, H. G., & Singh, V. (1994). Potential field tilt—A new concept for location of potential field sources. Journal of Applied Geophysics, 32(2–3), 213–217. https://doi.org/10.1016/0926-9851(94)90022-1.

[17]. Nabighian, M. N. (1972). The analytic signal of two-dimensional magnetic bodies with polygonal cross-section: Its properties and use for automated anomaly interpretation. Geophysics, 37(3), 507–517. https://doi.org/10.1190/1.1440276
[18]. Nigerian Geological Survey Agency. (2008). Geological map of Kabba Sheet 246 (1:100,000) [Map]. NGSA.
[19]. Nigerian Geological Survey Agency. (2010). Index map of airborne survey blocks flown between 2003–2010 by Fugro Airborne Services [Map]. NGSA.
[20]. Obaje, N. G. (2009). Geology and mineral resources of Nigeria. Springer.
[21]. Odeyemi, I. B. (1988). Lithostratigraphic and structural relationships of the upper Precambrian metasediments in Igarra area, western Nigeria. In Precambrian geology of Nigeria (pp. 111–123). Geological Survey of Nigeria.
[22]. Pirajno, F. (2009). Hydrothermal processes and mineral systems. Springer.
[23]. Rahaman, M. A. (1988). Recent advances in the study of the basement complex of Nigeria. In Precambrian geology of Nigeria (pp. 11–43). Geological Survey of Nigeria.
[24]. Reeves, C. (2005). Aeromagnetic surveys: Principles, practice and interpretation. Geosoft.
[25]. Roest, W. R., Verhoef, J., & Pilkington, M. (1992). Magnetic interpretation using the 3-D analytic signal. Geophysics, 57(1), 116–125.
[26]. Salem, A., Williams, S., Fairhead, D., Smith, R., & Ravat, D. (2008). Interpretation of magnetic data using tilt-angle derivatives. Geophysics, 73(1), L1–L10. https://doi.org/10.1190/1.2799992
[27]. Tawey, M. D., Alhassan, D. U., Adetona, A. A., Salako, K. A., Rafiu, A. A., & Udensi, E. E. (2020). Application of aeromagnetic data to assess the structures and solid mineral potentials in part of North Central Nigeria. Journal of Geography, Environment and Earth Science International, 24(5), 11–29.
[28]. Telford, W. M., Geldart, L. P., & Sheriff, R. E. (1990). Applied geophysics (2nd ed.). Cambridge University Press.
[29]. Verduzco, B., Fairhead, J. D., Green, C. M., & MacKenzie, C. (2004). New insights into magnetic derivatives for structural mapping. The Leading Edge, 23(2), 116–119.
[30]. Wilford, J. R., Bierwirth, P. N., & Craig, M. A. (1997). Application of airborne gamma-ray spectrometry in soil/regolith mapping and applied geomorphology. AGSO Journal of Australian Geology and Geophysics, 17(2), 201–216.